



## PAPER

[View Article Online](#)  
[View Journal](#) | [View Issue](#)Cite this: *Sustainable Energy Fuels*,  
2023, 7, 769Chemical insights into the base-tuned  
hydrothermal treatment of side stream biomasses†Vitalii Tkachenko,<sup>a</sup> Nader Marzban,<sup>ab</sup> Sarah Vogl,<sup>c</sup> Svitlana Filonenko <sup>\*a</sup>  
and Markus Antonietti <sup>a</sup>

Herein, we analyzed the hydrothermal processes applied to four very different side stream biomasses (chestnut foliage, sugar beet pressing chips, pine bark and branches from park cleaning, bamboo cuts) and identified diverse soluble products depending on the starting pH of the reaction, covering mild to strong basic pH conditions. Despite the biological diversity of the starting products, hydrothermal disintegration of biomass results in a remarkable reduction of chemical diversity towards a controllable number of molecular products, and the well-resolved and rather simple NMR-spectra allow the assignment of the products to only a few families of compounds. It has been revealed that in comparison with the classical hydrothermal treatment, where mostly hydrochar is produced, molar excess of base shifts the hydrothermal treatment towards a humification process. A further increase of the base content causes destruction of the biomass into the more oxygenated homogeneous colloid and thus, for the first time, it can be assigned to the hydrothermal fulviculation process. We discuss diverse valorization schemes depending on the biomass and conditions applied.

Received 30th October 2022  
Accepted 19th December 2022

DOI: 10.1039/d2se01513g

[rsc.li/sustainable-energy](https://rsc.li/sustainable-energy)

## Introduction

The time of fossil carbon sources to support chemistry is slowly running out,<sup>1</sup> and plant or microbial biomasses can become a renewed source of carbon fragments, being based only on light and CO<sub>2</sub>.<sup>2</sup> To begin, this is how fossil energy carriers were generated by natural processes on geological timescales, and this is also how they can be made in future, preferably by engineering processes.<sup>3</sup> The current white biotechnologies of bioethanol production<sup>4–6</sup> or biogas fermentation<sup>6–8</sup> are just two well-known examples, but in both cases, the efficiency for full biomass is comparably low,<sup>9</sup> e.g., methanization is rather incomplete, and larger amounts of the originally contained carbon are left over as fermentation sludges. Thermal gasification of biomass works only with dry, clean, high-value biomass and also shows relatively low conversion and energy yields, caused by the thermodynamic detour involving C=O as a defined intermediate.<sup>10</sup> Hydrothermal techniques, such as hydrothermal carbonization<sup>11,12</sup> or hydrothermal humification, have the advantage to work with wet or colloidal biomasses (such as sludges), and as optimized engineering processes

accelerated by increased temperature and pressure, they are much faster than biological or geological processes.<sup>13</sup> In addition, majority products are either in dissolved form or grained as humic substance or biochar, both with direct usage cascades. The clear processing advantages for biomass treatment and its applications for sustainable and efficient agricultural practices enabled IUPAC to name artificial humic matter within the Top Ten Emerging technologies.<sup>14</sup>

Any successful valorization scheme, in given chemical limits, should be only weakly dependent on the source of biomass, and especially local variations of soil, temperature, water, or climate should hardly be reflected in the chemical product. The amount of base in hydrothermal treatment tunes the process in wide ranges of chemical products and their diversity.<sup>15,16</sup> Molar base-to-biomass ratios result in the production of artificial humic substances – an emerging technology for carbon dioxide sequestration and an efficient soil amendment.<sup>17,18</sup> Despite wide interest in the scientific community, the chemistry behind the hydrothermal humification of a variety of biomasses is poorly discussed.

It is one purpose of the present paper to analyze how much product diversity and usage schemes depend on the biological diversity and the treatment processes involved. The base content is varied in a broad range to connect the two extreme cases: hydrothermal humification (excess amounts of base) and hydrothermal carbonization (mild base). The amounts and types of soluble fragments and solid products were then analyzed. On the other hand, we selected typical Central European biomasses, but concentrated on the side streams:

<sup>a</sup>Max-Planck Institute of Colloids and Interfaces, Department of Colloid Chemistry, Am Mühlenberg 1, 14476 Potsdam, Germany. E-mail: Svitlana.Filonenko@mpikg.mpg.de<sup>b</sup>Leibniz Institute of Agricultural Engineering and Bio-economy e.V. (ATB), Max-Eyth-Allee 100, 14469 Potsdam, Germany<sup>c</sup>Department of Chemistry, Functional Materials, Technische Universität Berlin, Hardenbergstrasse 40, D-10623 Berlin, Germany† Electronic supplementary information (ESI) available. See DOI: <https://doi.org/10.1039/d2se01513g>

- Chestnut foliage as a local variant of a yearly collected biomass stream from parks and inner cities.
- Sugar beet pressing chips as a side product of saccharose production.
- Pine bark and branches from park cleaning and as a side product of wood and paper production.
- Bamboo cuts as an example for one-year cultivation, lignocellulosic energy plants.

Based on the identified chemical structures and properties, we also discuss potential usage schemes for the products generated under the hydrothermal treatment with various amounts of base.

## Results and discussion

### Results of pH variation on biomass transformations

As a very lignin-rich waste biomass, we analyzed chestnut tree foliage from the park of Sanssouci, here infected by *Gracillariidae*. For preservation of plant health, these leaves have to be collected and burned, an energy-demanding process that returns the carbon stored in leaves back to the atmosphere. According to the analysis, they contain 42 wt% of cellulose, 39 wt% of lignin/tannins, with the remaining 19 wt% being mostly hemicellulose and waxes. The samples were hydrothermally treated as described in the experimental part, while the base content was varied between  $X = 0.25$ –5, with  $X$  being the molar ratio of the base to the assumed sugar units.

A visual overview of the products is given in Fig. 1. High amounts of base resulted in dark-brown, non-sedimenting dispersions with a minor amount of black precipitate, presumably insoluble parts of lignin mixed with minerals. The dispersion is stable upon storage. The final pH is still in the weakly alkaline region (pH = 8.5 at a five-fold excess (further VT500), see Table S1† for VT500 run), but far from the original ultrabasic starting solution.

A medium amount of base results in neutral pH values at the end of the reaction, with no clear sedimentation behavior, but increased amounts of a soft precipitate. A minor amount of base results in the classical hydrothermal carbonization behavior that is a well-defined sedimentation of a solid hydrochar phase from a yellow to orange overlayer medium with a clear, solely molecules-containing solution. It is obvious that the colloidal stability is related also to the final pH, *i.e.*, polymers and particles are potentially stabilized by ionized carboxylates and phenolates, which occur only at alkaline pH. We enhanced the sedimentation of the fraction composed of large solid particles by centrifugation (Fig. 2a), and analyzed the amount of carbon

and inorganic components in both solution (Fig. 2b) and centrifuged sediment (Fig. 2c) by weight. The results are presented as TIC and TOC diagrams.

The ash content in collected leaves is typically very high. This is related to the accumulated mineral dusts throughout the year, as well as the adhered soil grains from collecting the leaves in fall. In all cases, the liquid and solid yields are substantial. They require different treatments and analysis schemes, but the general trend is that more base generates more liquefied biomass products (Fig. 2d).

The sequestration and distribution of the carbon between solid and liquid phases after hydrothermal treatment with various amounts of the base depend on the cascade of the transformations that small molecular weight products from the biomass hydrolysis undergo. A basic pH condition prompts hydrolysis of the holocellulose, and glucose is the predominant starting molecule in the reaction mixture concerning biomass hydrothermal treatment. This work will concentrate on interpreting the mechanisms that glucose undergoes in the overheated water depending on the starting pH. Detected intermediates and hydrolysis products from other biomass components and their roles in chemical transformations towards final products will be explained. The main small molecular weight molecules are still presented in the reaction mixture after the end of the process, and can be detected by liquid NMR and HPLC. The NMR spectra of the lyophilized liquid phase (see Fig. 3a) form distinctive product patterns of the intermediates, which enables the discussion of the biomass transformation and resulting products to be divided into three rough groups: I – lack of KOH (VT025 and VT050), II – mild amount of KOH (VT100, VT150 and VT200) and III – excess of KOH (VT500), as summarized in Table S1.† The carbohydrate content has been calculated according to VDLUFA (2012; methods 6.5.1, 6.5.2 and 6.5.3).<sup>19</sup>

The group I corresponds to a process similar to a typical classical hydrothermal carbonization (HTC). Low amounts of base are consumed very fast at the beginning of the hydrothermal process. Thus, only a limited amount of carbohydrates can undergo retro-aldol addition towards lactic acid, products of its oxidative cleaving and organic acids formed from other intermediates.<sup>11</sup> The sample with the lowest base-to-biomass ratio is a typical product of the hydrothermal carbonization, considering both visual appearance and results from the CHN analysis (see Table 1), and SEM imaging (see Fig. 8). The base content is not enough to have any considerable influence on the acid-catalyzed dehydration and polycondensation of carbohydrates towards biochar. Fast precipitation of the product and the clear transparent supernatant point to complete product separation and only slight effects due to colloidal stability. Broad signals on NMR (see Fig. 3a) and FTIR spectra (see Fig. S1a†) also evidence the highly condensed polymeric structures, mostly in the region between 3 and 4 ppm. Those are the remaining partly etched cellulose fragments in the continuous phase as the most stable part of biomass under those conditions.<sup>20</sup> The amount of KOH is not enough to prohibit the fast drop of pH towards acidic region, and the forming furfural derivatives quickly condense into a highly cross-linked



Fig. 1 A line-up of the reaction mixtures after hydrothermal processing after 1 day of storage at room temperature.



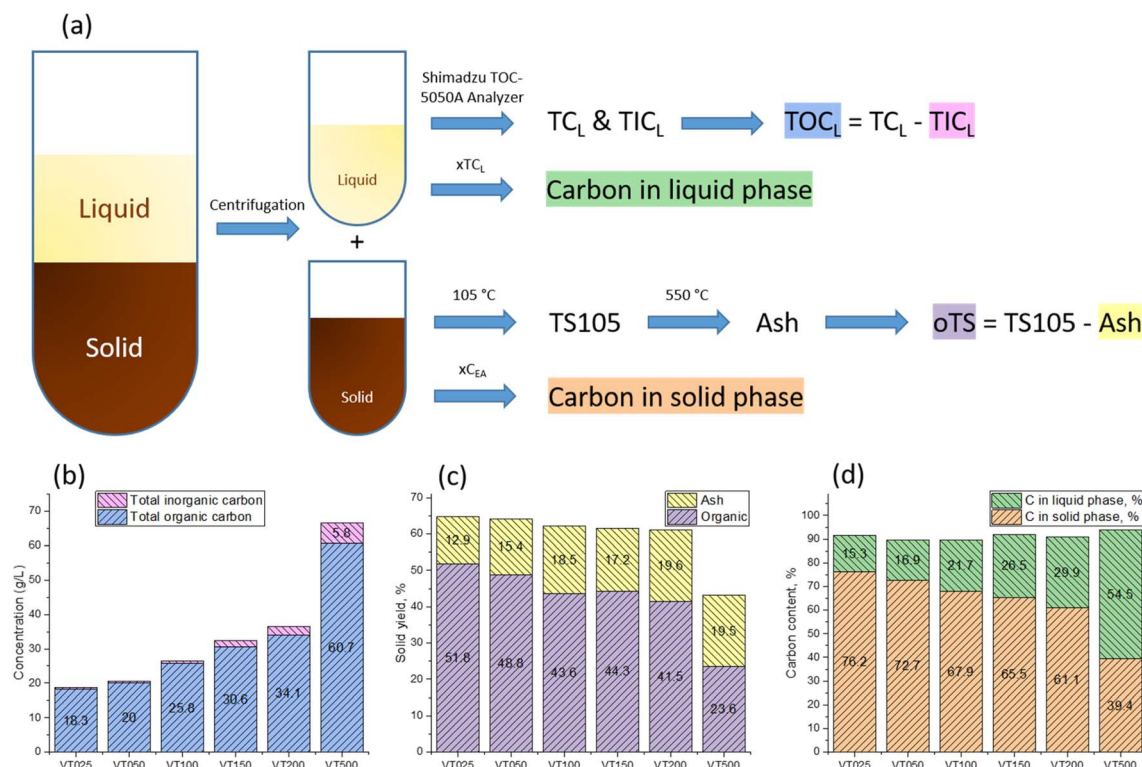


Fig. 2 (a) Separation procedure of the performed runs: phase unstable products of each run were separated from dissolved and dispersed products by centrifugation. (b) Concentration of carbon in the liquid/colloidal phase. In a liquid phase, the total carbon ( $TC_L$ ) and total inorganic carbon ( $TIC_L$ ) were determined and the total organic carbon ( $TOC_L$ ) was calculated by subtraction. (c) Yield of solid products (amount of biomass converted to solid fraction). (see the details of analysis in ESI†). (d) Carbon distribution in liquid/colloidal and solid phases after the hydrothermal process.

carbonaceous material. This explains the absence of the typical furfural derivative aromatic protons that occur at 7.5–6.5 ppm. In contrast, the NMR spectra in the range from 4.0 to 3.0 ppm reveal an abundance of oxygenated aliphatic protons, which are typical for the intermediate products (blue frame on Fig. 3b) of carbohydrate dehydration. There are only weak signals above 6 ppm. This suggests that the solution is almost free of double bonds and phenolates, which accumulate in the solid counterphase. This observation is also corroborated by HPLC employed for quantitative determination of the phenols content, furfurals, glucose and organic acids in the reaction media after hydrothermal processes from chestnut foliage (Fig. 4). On average, a  $2\times$  higher phenol derivative concentration was determined for the solid phase ( $\sim 0.2$  wt%) compared to the liquid/colloidal compartments ( $\sim 0.1$  wt%) (Fig. 4a and b). As a consequence, the amount of the aromatic compounds in the liquid phase is extremely low for detection by NMR. We also found furan derivatives (Fig. 3b green frame) at equilibrium concentrations for the solid and liquid fractions determined by HPLC. The absence of signals at 7.5 to 6.5 ppm specific to these molecules is due to the low residual pH and rapid condensation during the preparation of the NMR sample.

With the intermediate amount of base (group II), the organic acid diversity and the carbohydrate part of the NMR spectrum remain – with minor shifts – unchanged, but with increased intensities from 1 to 2.5 ppm. This happens because the retro-

aldol splitting of sugars and the consecutive hydride shift both preferably take place under alkaline conditions, resulting in the main products of lactic acid (a C3-acid), succinic acid (a C4-acid), and formic acid (C1) formation. As a result, the amount of organic acids increases (Fig. 3c and d), while the stronger KOH significantly decreases the size of the carbohydrate fragments (as indicated by a smaller, oligomer like peak broadening). New well-defined peaks at 4.5 ppm (an aromatic hydroxymethyl group, as the one of HMF), 7.3 ppm (furan), and 8.6 (proton at highly carboxylated aromatics) appear, indicating that the solution phase starts to accumulate a larger amount of furan derivatives. The final pH in these runs is 5.65, 6.80 and 7.26 (VT100, VT150 and VT200, respectively). Under these reaction conditions, the furfural derivatives formed in the final acidic media and formaldehyde groups are only partly subjected to condensation reactions, resulting in the less cross-linked, fluffy artificial humic polymer observed in the samples VT100, VT150 and VT200. Some amount of the preformed furan derivatives cannot condense due to insufficient acidity, appearing in the NMR spectra after the reaction and detectable with HPLC (Fig. 4a and b). Lignin degradation is also less expressed because of the increased pH, and this was confirmed by both NMR and HPLC techniques. All spectroscopic attributes of the group II samples point to a hydrothermal humification process characterized by the balance between the retro-aldol addition reaction of carbohydrates to organic acids and



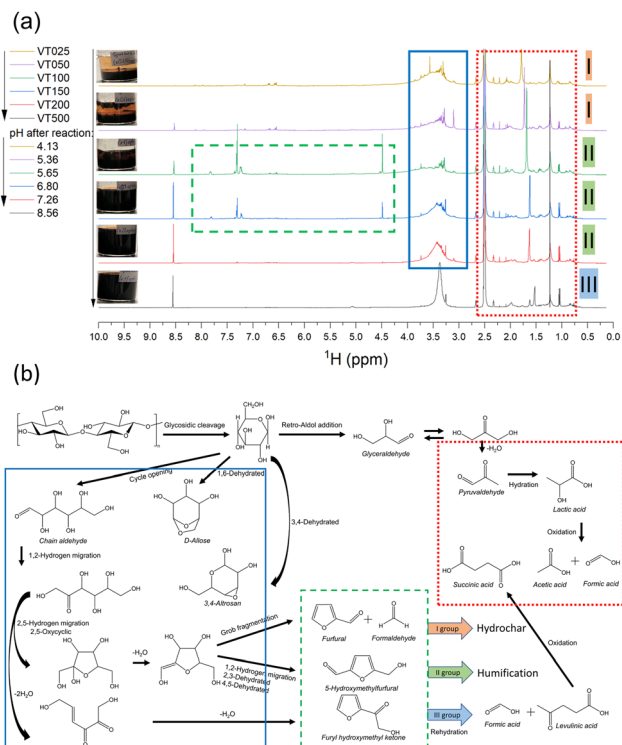


**Fig. 3** (a)  $^1\text{H}$  NMR spectra of the soluble products of chestnut foliage after hydrothermal treatment in the presence of various amounts of base: x0.25 eq. KOH  $\rightarrow$  1 – x5 eq. KOH (VT025  $\rightarrow$  VT500) with regard to the carbohydrate content in the starting biomass material. (b) Proposed degradation pathways of chestnut foliage via base-catalyzed retro-aldol addition and acid-catalyzed dehydration as pH dependent hydrothermal treatment. The different reaction pathways (b) can be followed by the different regions and groups on the NMR spectra (a) highlighted with corresponding frames. Blue frame – cellulose fragments, green-dashed frame – furan derivatives, red-dotted-frame – aliphatic compounds and organic acids.

**Table 1** N/C/H/O analysis data of the freeze-dried products of hydrothermal treatment in the presence of different amounts of KOH

Sample	N in %	C in %	H in %	O in %	O/C	H/C
Chestnut foliage	0.77	46.64	5.81	40.07	0.64	1.49
VT025	1.15	58.28	5.09	27.04	0.35	1.05
VT050	1.10	55.96	5.10	27.37	0.37	1.09
VT100	1.09	54.09	5.06	31.30	0.43	1.12
VT150	1.04	52.68	5.00	32.77	0.47	1.14
VT200	1.02	49.44	4.82	32.52	0.49	1.17
VT500	0.65	45.12	4.48	34.48	0.57	1.19

a consecutive dehydration-condensation reaction at slightly acidic pH. Under those conditions, the system avoids rapid condensation into a highly cross-linked carbonaceous material. Instead, linear or slightly branched humic polymers abundant in phenolates and carboxylic acids form, as easily judged by macroscopic observation and colloidal nature of the main product.

The group III at high base is finally practically free of any precipitates, and the products remain in the liquid phase

largely as organic acids, whose concentrations at least double. The base is not used up completely as evidenced by the high pH remaining after the reaction. Nearly all NMR signals are below 4 ppm, and the final peak at 8.56 ppm is typical for protons with highly carboxylated aromatics. The group III thereby demonstrates another scenario of the hydrothermal process. The excess of alkali allows for almost complete conversion of the carbohydrates towards the final products following the retro-aldol reaction. Even after exhaustion of all available carbohydrates, some alkali remains, resulting in a final pH value of 8.6. Ketone and aldehyde groups are of particular interest for possible further reactions, such as pyruvaldehyde, levulinic acid, glyceraldehyde. Here, the base-catalyzed aldol condensation occurs with the formation of linear well-soluble polymeric structures called fulvic acids. The decreased intensity of the signal at 8.56 ppm at maximum KOH proves the ongoing aldol re-condensation at alkaline pH, which is absent at neutral pH. Furanes are absent (because acidic pH values are never attained during the hydrothermal process), as confirmed by both NMR and HPLC techniques, due to the complete conversion towards organic acids and aldehydes. We might thereby call the III group – hydrothermal fulvic acid.

Most of the well-defined signals are in the region below 3 ppm, and correspond to a diversity of organic acids, keto- and hydroxyl acids (Fig. 3, red frame). Fig. 4c and d provide information about some organic acid final concentrations after the hydrothermal treatment. The acetic acid concentrations in both solid and liquid fractions remain constant at different KOH amounts, which underlines our assumption that it is mostly generated by ester splitting from acetylated hemicellulose and lignin.

The  $^{13}\text{C}$  CPMAS NMR spectra of VT050, VT150 and VT500 were measured (1 sample for each group) in order to evaluate the chemical structure of the humic substance in the solid phase (see Fig. 5). The signal at 182 ppm corresponds to the carbonyl carbon attached to the aromatic systems in highly substituted polymer systems. The sharpening signals reveal the formation of less crosslinked matter from VT050 to VT500, as a consequence of the higher mobility of different compartments presented in the samples when going from biochar (VT050) to humic substances (VT150 and VT500). The sharp peak at 168 ppm for the biochar sample can be attributed to the carbonyl group in the molecular state of the furan derivatives adsorbed on the biochar surface. This was also confirmed by HPLC study (Fig. 4a), where HMF and furfural were detected for VT050.

Phenolic aromatic groups found at 140 to 160 ppm for runs VT050 and VT150 are clearly detectable for these runs with HPLC and NMR studies. The resonance shown along the aryl-C region (110–140 ppm) originate from the condensed aromatic moiety units derived from lignin. The region from 0 to 45 ppm includes the alkyl-C signals assigned to the aliphatic chains of various lipid compounds, such as fatty acids and plant waxes.<sup>21</sup> The sharp bands around 29 ppm are related to the large abundance of bulk methylene segments of different molecules with specific structural conformation and rigidity, such as wax and cutin components. The identification of the molecular



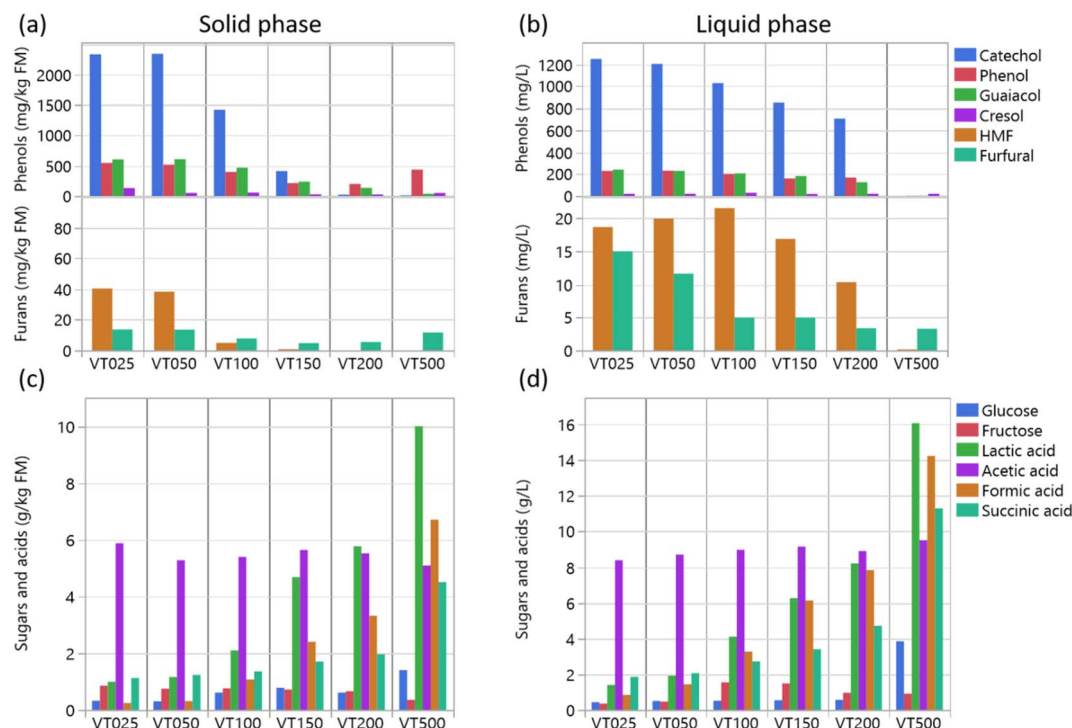


Fig. 4 Content of phenols, furfurals, glucose and organic acids in products of the hydrothermal process of chestnut foliage at different eq. KOH determined with HPLC. (a) Phenol and furfural derivatives in the solid fraction. (b) Phenol and furfural derivatives in the liquid fraction. (c) Glucose and organic acids in the solid fraction. (d) Glucose and organic acids in the liquid fraction.

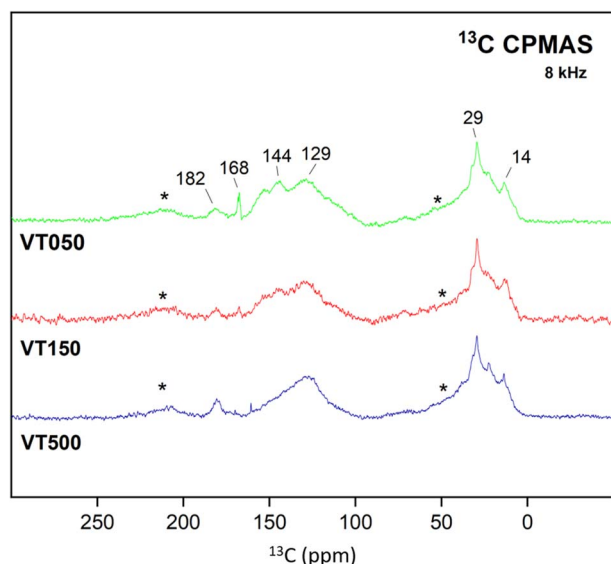


Fig. 5  $^{13}\text{C}$ -CPMAS-NMR spectra of the chestnut foliage solid phase after hydrothermal treatment. One sample for each group was measured.

species also allows for the explanation of simple sum analyses, such as elemental analysis, presented in Table 1. Generalized data are also presented in the van Krevelen diagram (see Fig. 6, hydrochar zone according to ref. 22), representing the composition in ratios of H/C and O/C. We see that low base

hydrothermal processes really progress along the previously described HTC path: the biomass mostly splits with water by dehydration, and the overnight reaction results in a lignite-like product (longer reaction times and higher temperatures cause black coal compositions).<sup>23–25</sup> The decrease of nitrogen content in the solid phase was observed for the VT500 run, where the reaction mixture possesses basic pH at the end of the process. This pH avoids protonation of amino groups, and as a consequence, poor adsorption on negatively charged sediments occurs. Furan derivatives, as supported by the NMR data, undergo splitting to carboxyl acids, which then undergo aldol condensation with less water elimination. We also applied HSQC to confirm our assignments. (Owing to the transfer to non-expert labs, an additional decline of the hydrogen content

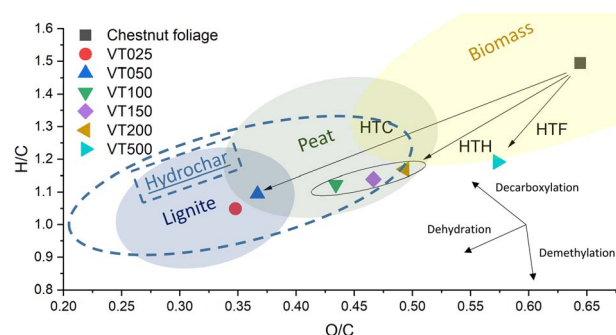


Fig. 6 Van Krevelen diagram of the products of hydrothermal treatment of chestnut foliage based on elemental analysis.

is typical for lignin-rich products. This is attributed to a demethylation of the coniferyl and sinapyl alcohol upon creation of methanol, which is also obtained by the dry distillation of wood as “wood spirit”. Splitting up the reaction path in the van Krevelen diagram into a dehydration and demethylation path allows for the estimation of the degree of demethylation. Furthermore, alkaline treatment splits up the available methoxy groups, so we intend to keep discriminative analysis as simple as possible, at the best with tabletop machines). Two of these spectra are shown in Fig. 7a and b for the VT150 and VT500 runs, respectively. These spectra essentially confirm our previous assignments, but also reveal some further details of the mechanism. We see a strong signal for acetate groups in both samples, which we attribute to the former acetylation of hemicellulose and lignin. Another point is the formation of terminal methyl groups, which give weak signals under acidic conditions and presumably only related to the wax content, while their increase under alkaline conditions clearly proves the occurrence of an alkaline hydride shift, *e.g.*, from glyceraldehyde to lactic acid. In the better resolved 2D spectra, we also found indications of lignin or tannin degradation towards soluble fragments.

### The disperse/solid phase

Discussing the NMR spectra and considering the heterogenous nature of the samples, it is clear that we up to now analyzed the soluble species with sufficient mobility. For instance, even the supernatants are completely non-transparent for group III of the hydrothermal process (see Fig. 1), pointing to the excellent efficiency of the high charges of fulvic species to stabilize colloids made up from non-soluble species. As the amount of phenols is very high in chestnut foliage, and they were only a small amount of phenols in the NMR spectra, the mass balance between the two phases suggests they are mostly in the heterogeneous particles. SEM images, also coupled to EDX (see Fig. S2† for solid phase and Fig. S3† for dispersion), allowed us to study the structure and the relative specific surface area of the solid phase (Fig. 8). At highest base (Fig. 8a), the structure is the one of the mineral impurities and inclusions, coated with

a phenolic layer. In group II with the relative balance of base and biomass sugar, the structure is very different, fluffy and full of structural pores, indicating a low interface energy towards water (Fig. 8b–d). This is the typical, well reported texture of humic acid/clay conjugates,<sup>26,27</sup> *i.e.*, we are in the hydrothermal humification range. At lower base, the transition to hydrothermal carbonization is observed (Fig. 8e and f). According to the lower ionic content and stabilization, the structures are denser, still created from primary carbon nanoparticles, but in a tighter packing orientation and with stronger connections between the particles. We assume these high colloidal surface areas to be loaded with solution species, bound by adsorption.

### Variation of biomasses

To obtain a more general sense of the observations, we also analyzed three other types of side stream biomasses available in large amount, among them forestry remnants (multiple years grown, high in phenols and minerals), bamboo chops (one year-lignocellulosic biomass rich in waxes, a model also for corn stalks, sugar cane bagasse, or miscanthus), and sugar beet remnants (soft industrial side biomass from food production) treated in the hydrothermal humification regime. The NMR spectra of the soluble species are shown in Fig. 9, while the FTIR spectra are shown in Fig. S1b.† The pH values of the final reaction mixtures were all close to neutral (pH = 6.48–6.80), *i.e.*, the reaction progressed in a similar manner, independent of the specific plant textures. Despite the high biological diversity, the spread of chemical products is practically the same. All signals appeared with slightly different intensities at the same positions, and the biological effects were reduced to a clearly increased alkyl fraction from bamboo, while bark and branches seem to be more easily digestible (as judged by the relative narrow carbohydrate leftover peak). The FTIR spectra are also very similar, except for an amide peak found only in the sugar beet product (sugar beet contains about 10 wt% of protein in the raw biomass before saccharose extraction. This is different from the other biomasses).

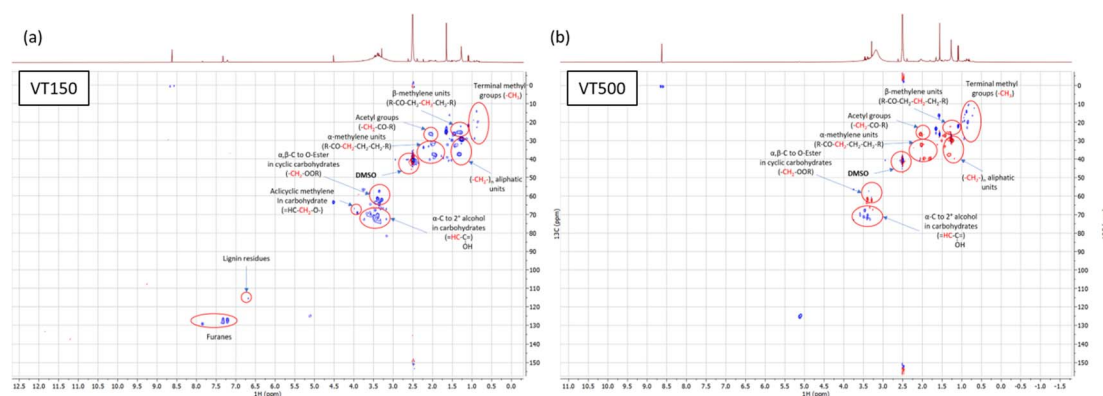


Fig. 7 (a) 2D  $^1\text{H}$ – $^{13}\text{C}$  HSQC NMR (two-dimensional  $^1\text{H}$ – $^{13}\text{C}$  gradient heteronuclear single quantum coherence nuclear magnetic resonance NMR) spectra of hydrothermal treatment sample VT150. (b) 2D  $^1\text{H}$ – $^{13}\text{C}$  HSQC NMR (phase sensitive:  $-\text{CH}_2-$  opposite phase (red) than  $-\text{CH}-$  and  $-\text{CH}_3$  (blue)) spectra of the hydrothermal treatment sample VT500.





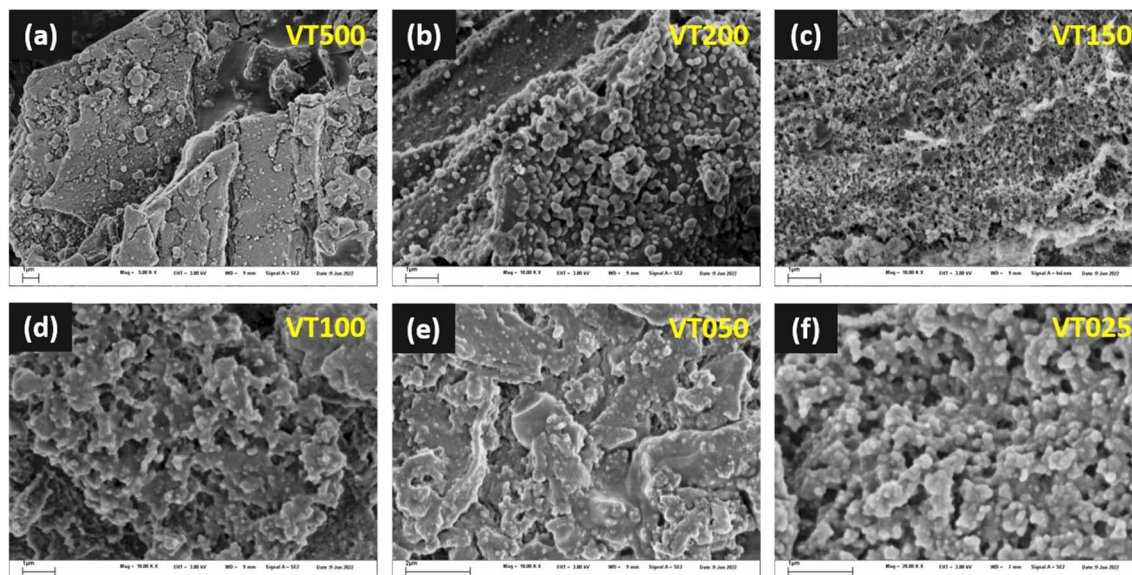


Fig. 8 SEM images of the chestnut foliage solid fraction after hydrothermal treatment at different amounts of KOH. (a) Hydrothermal fulvication (group III); (b)–(d) hydrothermal humification (group II) and (e and f) hydrothermal carbonization (group I).

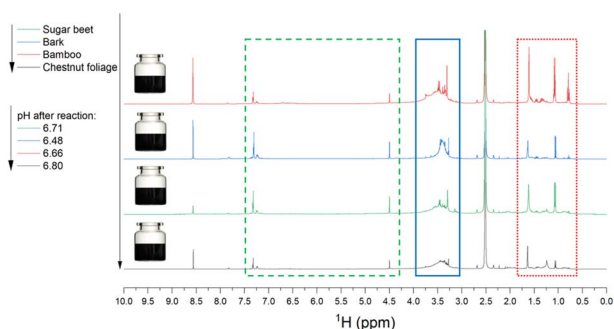


Fig. 9  $^1\text{H}$  NMR of hydrothermal humification based on different biomasses: sugar beet, bark, bamboo and chestnut foliage at  $\times 1.50$  eq. KOH. Blue frame – cellulose fragments, green-dashed frame – furan derivatives, red-dotted-frame – aliphatic compounds and organic acids.

We take all of these results as an indication to claim the hydrothermal biomass conversion in a first approximation independent of the specific biomass origin.

### Usage schemes for the converted chemical products

To discuss the potential usage and valorization schemes of the converted products, we have to quantify the content of specific chemicals in both solid and liquid fractions. For that, we utilize the abovementioned quantitative HPLC for hydrothermal mechanism interpretation.

Fig. 4a and b illustrate the general trend of phenols content, which significantly decreases with the increase of KOH. Within VT025 to VT100, the hydrothermal process finishes under an acidic condition, where a part of lignin undergoes Friedel–Crafts dealkylation more efficiently towards phenols. Thus, catechol is detected as the main phenolic product in both solid and liquid fractions. We have to underline that catechol

equilibrates between the solid and liquid phases. Thus, by weight, a larger amount already stays bound at the solid phase, with decreasing solid content being adsorbed less. Phenol and guaiacol are both produced in lower amounts with almost equal concentrations over the whole range of studied KOH content. For VT150 to VT500, the overall concentration of phenol derivatives drastically decreases, *i.e.*, we indeed required acidic conditions to liberate the phenols, or *vice versa*, alkaline media is necessary to achieve the absence of phenols. Fig. 4a and b also report the concentration of furfural and HMF in the solid and liquid phases, respectively. As furans usually come with distinct regulatory issues, it is preferable that their concentration remains low. On the other hand, HMF in honey and fruit jams can be notoriously high, and sugarcane molasses can easily contain 100–300 mg HMF per kg.<sup>28</sup> The reported values here are significantly smaller, but worth the consideration for agricultural applications.

Fig. 4c and d provide information about some organic acid final concentrations after hydrothermal treatment. Acetic acid concentrations in both solid and liquid fractions remain constant at different KOH amounts, which was attributed to ester splitting from acetylated hemicellulose and lignin. The acetic acid content is about 1 wt% overall, which is rather high. The overall concentration of organic sugars (fructose and glucose) and acids (lactic acid (a C3-acid), succinic acid (C4), and formic acid (C1)) at high base is found to be around  $65 \text{ g L}^{-1}$  of the liquid reaction fluid, with another  $28 \text{ g kg}^{-1}$  adsorbed onto the solid sediment.

The use of the artificial humic acid mixture in group II or the processes has already been discussed in the literature.<sup>29–31</sup> Indeed, the promotion of soil quality, microbiome growth and improvement of agronomical indices to increase grain yield was proven most times. This is in part also true for the hydrochar generated in group I,<sup>32</sup> as polar digestible molecules are



generated here. However, the furan derivatives content might be inhibitive in the early phases of application.

What is left is the use of the high organic acid content generated in group III, which we called here simplistically hydrothermal fulvication. All of these organic acids represent value as such, but must then be isolated and separated. Using such mixtures for fermenters in white biotechnology however could generate a simpler usage strategy, for instance, calculated methanization yields of  $17 \text{ g L}^{-1}$  or  $24 \text{ m}^3 \text{ CH}_4$  per  $\text{m}^3$  digestate, which was by recipe 20 wt% wet biomass and 80 wt% of base/water.

## Conclusions

In this article, we compared three different hydrothermal digestion schemes tuned by the amount of the added base, and applied to four different agricultural side stream biomasses: chestnut foliage, side products of wood industry, bamboo chops as a typical one-year lignocellulosic harvest, and sugar beet pressing residues as a typical side product of food industry. Molar excess of base shifts the hydrothermal treatment towards a humification process, and further increase of the base content causes destruction of the biomass into a homogeneous colloid in a fulvication process.

Independent of the specific biomass starting products, the hydrothermal disintegrations are rather similar despite the chemical product spectra. Thus, the hydrothermal processes appear to be independent of the specific biology and textures. This is excellent news from an engineering perspective when the dissolved products are the focal point. The absence or minor addition of base or ashes results in an acid-catalyzed reaction cascade, running mostly along dehydration of the contained sugars and the formation of a typical HTC furanic hydrochar. The phenol-content can be rather high (up to  $5 \text{ g kg}^{-1}$ ) in this process, as lignin turns out to liberate monocyclic phenols by acid-catalyzed Friedel–Crafts dealkylation.

A process with applied medium base content results in hydrothermal humification. The reaction begins under alkaline conditions, but ends with weakly acidic conditions. Furthermore, the condensation products are more functional, highly hygroscopic, and much less cross-linked, while the furan derivatives and phenols play less of a role in the condensation and appear less in the products. The artificial humic acid prepared as such was already carefully analyzed as a soil additive, and both microbial and agronomic traits were found to be outstanding.<sup>33</sup>

We also found an all-alkaline path, referred as hydrothermal fulvication, practically free of phenols and furanes. The highest yields of organic acids are created under this conditions, namely increasing amounts of lactic acid (3 + 3 splitting), formic acid (5 + 1 and 1 + 4 + 1 splitting), and succinic acid (1 + 4 + 1, again). Acetic acid, present in the same amounts independent on the run, most likely is formed only by ester splitting of the contained acetates. As all these organic acids are also known to be products of fermentation processes,<sup>34</sup> we can consider the liquid phase as nutrition fluids for fermenters, such as in the

most simple case for accelerated and also yield-boosted biogas production.

## Author contributions

The manuscript was written through contributions of all authors. All authors have given approval to the final version of the manuscript.

## Conflicts of interest

There are no conflicts to declare.

## Acknowledgements

This research did not receive any specific grant from funding agencies in the public, commercial, or not-for-profit sectors. V. T., N. M., S. F. and M. A. gratefully acknowledge the Max Planck Society for financial support. S. V. is grateful for the funding by the Deutsche Forschungsgemeinschaft (DFG, German Research Foundation) under Germany's Excellence Strategy – EXC 2008–390540038 – UniSysCat. NM thank the German Academic Exchange Service (DAAD) for providing financial support and the analytical chemistry group (Leibniz Institute of Agricultural Engineering and Bioeconomy) for their expertise and support with the analytical techniques. Authors acknowledge Antje Voelkel for performing CHN analysis. Open Access funding provided by the Max Planck Society.

## References

- 1 K. S. Lackner, *Annu. Rev. Energy Environ.*, 2002, **27**, 193–232.
- 2 A. Miltner, P. Bombach, B. Schmidt-Brücken and M. Kästner, *Biogeochemistry*, 2012, **111**, 41–55.
- 3 R. J. Pearson, M. D. Eisaman, J. W. Turner, P. P. Edwards, Z. Jiang, V. L. Kuznetsov, K. A. Littau, L. Di Marco and S. G. Taylor, *Proc. IEEE*, 2011, **100**, 440–460.
- 4 A. K. Chandel, S. S. Da Silva and O. V. Singh, *BioEnergy Res.*, 2013, **6**, 388–401.
- 5 K. Kuroda and M. Ueda, *Biotechnol. Lett.*, 2011, **33**, 1–9.
- 6 A. Aguiar, T. S. Milessi, D. R. Mulinari, M. S. Lopes, S. M. da Costa and R. G. Candido, *Biomass Bioenergy*, 2021, **144**, 105896.
- 7 A. Pandey, R. Hofer, M. Taherzadeh, M. Nampoothiri and C. Larroche, *Industrial Biorefineries and White Biotechnology*, Elsevier, 2015.
- 8 M. A. Z. Coelho and B. D. Ribeiro, *White Biotechnology for Sustainable Chemistry*, Royal Society of Chemistry, 2016.
- 9 K. J. Ptasiński, M. J. Prins and A. Pierik, *Energy*, 2007, **32**, 568–574.
- 10 A. Demirbas, *Prog. Energy Combust. Sci.*, 2005, **31**, 171–192.
- 11 B. Hu, K. Wang, L. Wu, S. H. Yu, M. Antonietti and M. M. Titirici, *Adv. Mater.*, 2010, **22**, 813–828.
- 12 M.-M. Titirici and M. Antonietti, *Chem. Soc. Rev.*, 2010, **39**, 103–116.
- 13 F. Yang and M. Antonietti, *Prog. Polym. Sci.*, 2020, **100**, 101182.





- 14 F. Gomollón-Bel, *Chem. Int.*, 2021, **43**, 13–20.
- 15 Y. Cao, M. He, S. Dutta, G. Luo, S. Zhang and D. C. Tsang, *Renewable Sustainable Energy Rev.*, 2021, **152**, 111722.
- 16 S. K. Tiwari, M. Bystrzejewski, A. De Adhikari, A. Huczko and N. Wang, *Prog. Energy Combust. Sci.*, 2022, **92**, 101023.
- 17 C. Tang, B. Liu, K. Cheng, M. Antonietti and F. Yang, *Land Degrad. Dev.*, 2022, 1–11.
- 18 Y. Lan, S. Gai, K. Cheng and F. Yang, *Environ. Sci.: Water Res. Technol.*, 2022, 1173–1187.
- 19 Association of German agricultural inspection and research institute, [https://www.vdlufa.de/Methodenbuch/index.php?option=com\\_content&view=article&id=4&Itemid=111&lang=de](https://www.vdlufa.de/Methodenbuch/index.php?option=com_content&view=article&id=4&Itemid=111&lang=de), ch. 6.5.1–6.5.3, accessed December 2022.
- 20 R. Demir-Cakan, N. Baccile, M. Antonietti and M.-M. Titirici, *Chem. Mater.*, 2009, **21**, 484–490.
- 21 R. Spaccini, V. Cozzolino, V. Di Meo, D. Savy, M. Drosos and A. Piccolo, *Sci. Total Environ.*, 2019, **646**, 792–800.
- 22 A. Hornung, F. Stenzel and J. Grunwald, *Biomass Convers. Biorefin.*, 2021, 1–12.
- 23 M.-M. Titirici, A. Thomas and M. Antonietti, *New J. Chem.*, 2007, **31**, 787–789.
- 24 S. Nizamuddin, H. A. Baloch, G. J. Griffin, N. M. Mubarak, A. W. Bhutto, R. Abro, S. A. Mazari and B. S. Ali, *Renewable Sustainable Energy Rev.*, 2017, **73**, 1289–1299.
- 25 M. Heidari, A. Dutta, B. Acharya and S. Mahmud, *J. Energy Inst.*, 2019, **92**, 1779–1799.
- 26 C. Tang, Y. Li, J. Song, M. Antonietti and F. Yang, *Iscience*, 2021, **24**, 102647.
- 27 S. Zhang, J. Song, Q. Du, K. Cheng and F. Yang, *Chemosphere*, 2020, **250**, 126606.
- 28 P. Singh, R. H. Jayaramaiah, S. B. Agawane, G. Vannuruswamy, A. M. Korwar, A. Anand, V. S. Dhaygude, M. L. Shaikh, R. S. Joshi and R. Boppana, *Sci. Rep.*, 2016, **6**, 1–13.
- 29 S. Zhang, Q. Du, K. Cheng, M. Antonietti and F. Yang, *Chem. Eng. J.*, 2020, **394**, 124832.
- 30 F. Yang, C. Tang and M. Antonietti, *Chem. Soc. Rev.*, 2021, **50**, 6221–6239.
- 31 W. Huang, P. Wen, W. Wang, X. Liu, Y. Wang, Z. Yu, Y. Li, Y. Hou and S. Zhou, *J. Environ. Chem. Eng.*, 2022, 107985.
- 32 S. Steinbeiss, G. Gleixner and M. Antonietti, *Soil Biol. Biochem.*, 2009, **41**, 1301–1310.
- 33 Y. Yuan, S. Gai, C. Tang, Y. Jin, K. Cheng, M. Antonietti and F. Yang, *Appl. Soil Ecol.*, 2022, **179**, 104587.
- 34 J.-S. Lee, C.-J. Lin, W.-C. Lee, H.-Y. Teng and M.-H. Chuang, *Biotechnol. Biofuels Bioprod.*, 2022, **15**, 1–11.

